Effective connectivity differences in motor network during passive movement of paretic and non-paretic ankles in subacute stroke patients

Marianna Nagy [Corresp., 1] , **Csaba Aranyi** [2] , **Gábor Opposits** [2] , **Tamás Papp** [1] , **Levente Lánczi** [1, 3] , **Ervin Berényi** [1] , **Csilla Vér** [4] , **László Csiba** [4] , **Péter Katona** [3] , **Tamás Spisák** [5] , **Miklós Emri** [2]

[1] Faculty of Medicine, Department of Medical Imaging, Division of Radiology and Imaging Science, University of Debrecen, Debrecen, Hajdú-Bihar, Hungary

[2] Faculty of Medicine, Department of Medical Imaging, Division of Nuclear Medicine and Translational Imaging, University of Debrecen, Debrecen, Hajdú-Bihar, Hungary

[3] Department of Diagnostic Radiology, Kenézy University Hospital, Debrecen, Hajdú-Bihar, Hungary

[4] Clinical Center, Department of Neurology, University of Debrecen, Debrecen, Hajdú-Bihar, Hungary

[5] Department of Neurology, University Hospital Essen, Essen, Germany

Corresponding Author: Marianna Nagy
Email address: nagy.marianna@med.unideb.hu

Background: A better understanding of the neural changes associated with paresis in stroke patients could have important implications for therapeutic approaches. Dynamic Causal Modeling (DCM) for functional magnetic resonance imaging (fMRI) is commonly used for analyzing effective connectivity patterns of brain networks due to its significant property of modeling neural states behind fMRI signals. We applied this technique to analyze the differences between motor networks (MNW) activated by continuous passive movement (CPM) of paretic and non-paretic ankles in subacute stroke patients. This study aimed to identify CPM induced connectivity characteristics of the primary sensory area (S1) and the differences in extrinsic directed connections of the MNW and to explain the hemodynamic differences of brain regions of MNW. Methods: For the network analysis, we used ten stroke patients' task fMRI data collected under CPMs of both ankles. Regions for the MNW, the primary motor cortex (M1), the premotor cortex (PM), the supplementary motor area (SMA) and the S1 were defined in a data-driven way, by independent component analysis. For the network analysis of both CPMs, we compared twelve models organized into two model-families, depending on the S1 connections and input stimulus modelling. Using DCM, we evaluated the extrinsic connectivity strengths and hemodynamic parameters of both stimulations of all patients. Results: After a statistical comparison of the extrinsic connections and their modulations of the "best model", we concluded that three contralateral self-inhibitions (cM1, cS1, and cSMA), one contralateral inter-regional connection (cSMA→cM1), and one interhemispheric connection (cM1→iM1) were significantly different. Our research shows that hemodynamic parameters can be

estimated with the Balloon model using DCM but the parameters do not change with stroke. Conclusions: Our results confirm that the DCM-based connectivity analyses combined with Bayesian model selection may be a useful technique for quantifying the alteration or differences in the characteristics of the motor network in subacute stage stroke patients and in determining the degree of MNW changes.

1 # Effective Connectivity Differences in Motor Network
2 # During Passive Movement of Paretic and Non-Paretic
3 # Ankles in Subacute Stroke Patients

5 Marianna Nagy[1], Csaba Aranyi[2], Gábor Opposits[2], Tamás Papp[1], Levente István Lánczi[1, 4], Ervin
6 Berényi[1], Csilla Vér[3], László Csiba[3], Péter Katona[4], Tamás Spisák[5], and Miklós Emri[2]

8 [1] Department of Medical Imaging, Division of Radiology and Imaging Science, Faculty of
9 Medicine, University of Debrecen, Hungary
10 [2] Department of Medical Imaging, Division of Nuclear Medicine and Translational Imaging,
11 Faculty of Medicine, University of Debrecen, Hungary
12 [3] Department of Neurology, Clinical Center, University of Debrecen, Hungary
13 [4] Department of Diagnostic Radiology, Kenézy University Hospital, Debrecen, Hungary
14 [5] Department of Neurology, University Hospital Essen, Essen, Germany

16 Corresponding Author:
17 Marianna Nagy[1]
18 Department of Medical Imaging, Division of Radiology and Imaging Science, Faculty of
19 Medicine, University of Debrecen
20 98. Nagyerdei krt., Debrecen, Hajdú-Bihar, 4032, Hungary
21 Email address: nagy.marcsa@gmail.com

Abstract

23 **Abstract**
24 Background: A better understanding of the neural changes associated with paresis in stroke
25 patients could have important implications for therapeutic approaches. Dynamic Causal
26 Modeling (DCM) for functional magnetic resonance imaging (fMRI) is commonly used for
27 analyzing effective connectivity patterns of brain networks due to its significant property of
28 modeling neural states behind fMRI signals. We applied this technique to analyze the differences
29 between motor networks (MNW) activated by continuous passive movement (CPM) of paretic
30 and non-paretic ankles in subacute stroke patients. This study aimed to identify CPM induced
31 connectivity characteristics of the primary sensory area (S1) and the differences in extrinsic
32 directed connections of the MNW and to explain the hemodynamic differences of brain regions
33 of MNW. Methods: For the network analysis, we used ten stroke patients' task fMRI data
34 collected under CPMs of both ankles. Regions for the MNW, the primary motor cortex (M1), the
35 premotor cortex (PM), the supplementary motor area (SMA) and the S1 were defined in a data-
36 driven way, by independent component analysis. For the network analysis of both CPMs, we
37 compared twelve models organized into two model-families, depending on the S1 connections
38 and input stimulus modelling. Using DCM, we evaluated the extrinsic connectivity strengthsand
39 hemodynamic parameters of both stimulations of all patients. Results: After a statistical

40 comparison of the extrinsic connections and their modulations of the "best model", we concluded
41 that three contralateral self-inhibitions (cM1, cS1, and cSMA), one contralateral inter-regional
42 connection (cSMA→cM1), and one interhemispheric connection (cM1→iM1) were significantly
43 different. Our research shows that hemodynamic parameters can be estimated with the Balloon
44 model using DCM but the parameters do not change with stroke. Conclusions: Our results
45 confirm that the DCM-based connectivity analyses combined with Bayesian model selection
46 may be a useful technique for quantifying the alteration or differences in the characteristics of
47 the motor network in subacute stage stroke patients and in determining the degree of MNW
48 changes.
49
50 **Introduction**
51
52 Numerous studies have used functional magnetic resonance imaging (fMRI) to investigate neural
53 reorganization and functional recovery after stroke (Calautti et al., 2007). fMRI univariate
54 analysis of regional activation is valuable for understanding the regional neural substrates
55 associated with cognitive functions (Ma et al., 2015). Using active and passive motion-based
56 fMRI experiments (Lazaridou et al., 2013; Cheng et al., 2012) researchers have typified the post-
57 stroke motor dysfunction and the corresponding potential cerebral reorganization. In our
58 previous therapeutic study, we examined the effects of passive movement on blood oxygen level-
59 dependent (BOLD) responses in both hemispheres (Vér et al., 2016). Our results showed that
60 passive movement of the paretic ankle increased BOLD responses in the contralateral pre- and
61 postcentral gyrus, superior temporal gyrus, central opercular cortex, and in the ipsilateral
62 postcentral gyrus, frontal operculum cortex and cerebellum.
63 Various brain areas are responsible for the execution of movements: the primary motor cortex
64 (M1), supplementary motor area (SMA), and the premotor cortex (PM). The M1 controls the
65 execution of movement by generating neural impulses (Penfield & Boldrey, 1937) and the PM
66 regulates the initiation of different motion patterns (Hoshi & Tanji, 2000). The role of the SMA
67 is also planning movement, but this is an essential brain area that is activated even when the
68 motion is not performed, but we are only thinking about it (Tanji & Shima, 1994). These regions
69 create the motor network (Biswal et al., 1995) which is primarily responsible for conducting and
70 controlling a wide variety of movements (Lam et al., 2018).
71 In the literature, many researchers used fMRI to investigate the connections and connectivity
72 patterns amongst motor areas during active movement of paretic upper limb after stroke
73 compared to controls. These studies (Rehme et al., 2011; Bajaj et al., 2016) showed that task
74 demands alter the intensity and volume of brain activity and that these activation changes are
75 specific to certain brain regions.
76 Dynamic Causal Modeling (DCM) for fMRI is commonly used for analyzing effective
77 connectivity patterns of brain networks. The connection strength between brain regions is
78 assessed at the underlying neuronal level rather than the observed hemodynamic level (Friston,
79 Harrison & Penny, 2003). In DCM connectivity is expressed in Hz that shows the rate at which a

80 region's activity is mediated to another region that is directly connected to. DCM provides a fully
81 Bayesian framework to estimate the connectivity strengths of neural interactions between brain
82 regions as well as the regional self-inhibitory effects and regional hemodynamic parameters.
83 DCM considers several variables such as hemodynamic response, flow induction, activity-
84 dependent signal, change in volume and the level of deoxyhemoglobin. It uses the extended
85 Balloon model (Friston et al., 2000) to describe hemodynamic changes due to neuronal activity.
86 For studying the effective connectivity of several diseases DCM has been successfully used
87 (Seghier et al., 2010).
88 Cerebrovascular disorders may affect the shape of the hemodynamic response function (HRF) of
89 BOLD signal. In such patients, HRFs can have lower amplitudes, longer time to peak (TTP), and
90 deeper initial dips (Altamura et al., 2009; Roc et al., 2006). These observations were also
91 described in cases of retained neuronal activity (Binkofsk & Seitz, 2004; Röther et al., 2002) and
92 in relation to altered cerebral hemodynamics (Altamura et al., 2009; Hamzei et al., 2003),
93 suggesting that decreased BOLD signals might reflect the reduction of neuronal activation or be
94 the result of neurovascular uncoupling.
95 Our study investigates whether the impairment of cerebral hemodynamics in subacute stroke
96 patients is related to changes in the BOLD signal HRF.
97 Task-dependent effective connectivity among motor cortex regions has been documented at rest
98 and during whole-hand fist closing (Grefkes et al., 2008; Nowak et al., 2008). In able-bodied
99 individuals, the strength and sign of neural coupling between motor areas is modulated by the
100 task (i.e., rest, unilateral, bilateral).
101 Investigations from the upper limb suggest that the intensity and volume of activity in the
102 primary sensory and motor cortices (S1 and M1) and in the cerebellum are sensitive to
103 movement rate (Saleh et al., 2016). In contrast with M1, S1, and the cerebellum, the effect of
104 upper extremity movement rate is less robust in the premotor and supplementary motor areas
105 (PM and SMA, respectively) (Inman et al., 2012). Less is known about the brain activation
106 pathway changes during continuous passive movement (CPM) of a lower extremity.
107 Observations from the upper limb provide a framework for understanding how brain activity
108 changes across different lower limb movement tasks. However, whether upper and lower limb
109 movements are similarly controlled with respect to rate and complexity remains unclear because
110 few studies have examined this issue during tasks of the lower limbs (Vinehout, Schmit &
111 Schindler-Ivens, 2019). Differences in the characteristics of arm and leg movements suggest that
112 supraspinal control may also be different (Mehta et al., 2012; Cleland & Schindler-Ivens, 2018).
113 Many DCM studies aimed to find the best model for the motor network (Volz et al., 2015;
114 Diekhoff-Krebs et al., 2017) and in most cases, the best model was the fully connected model.
115 For the upper limb, Rehme et al. (Rehme et al., 2011) investigated the temporal evolution of
116 intra- and interhemispheric connectivity during motor recovery from the acute to the early
117 chronic phase post-stroke. They analyzed 17 possible models and found the fully connected
118 model provided the best results through groups and series. In a similar study, Bajaj et al. studied
119 the connectivity pattern of the motor network in the affected and unaffected hemisphere during

120 finger-tapping task with healthy and paretic arms (Bajaj et al., 2016). From the eight defined
121 connectivity models, they found that the full model fitted the measured data well in the affected
122 hemisphere when the task was completed by the affected hand. In similar research, Volz et al.
123 (Volz et al., 2015) compared the changes in motor network connectivity during upper and lower
124 limb motion. They examined 39 models and also found that the best was the fully connected
125 model. In contrast, we defined model families depending on the external stimulus and the
126 connectivity patterns of the S1 region and use the Bayesian model selection technique, which
127 provides evidence for one model over other based upon evidence ratios (i.e., Bayes factors) or
128 differences in log evidence (Congdon, 2007).
129 In our previous publication (Aranyi et al., 2017), we examined potential sources of systematic
130 motion artefacts in stroke using fMRI concentrating on those causing stimulus-correlated motion
131 on the individual-level and separated the motion effect change on the fMRI signal from the
132 activation-induced modification at the population level. To allow the models accounting for the
133 sensory dimension of CPM (sensory-feedback), we added the S1 and designed model families to
134 map its connectivity pattern to the motor system.
135 The aim of the study was to examine the motor network and the connectivity differences in both
136 hemispheres during continuous passive movement (CPM) of non-paretic and paretic ankles in
137 subacute stroke patients in the context of the neuroanatomical and functional background. We
138 specifically focused on the role of the S1 within the network and investigated these modified
139 networks' connectivity differences during CPM of non-paretic and paretic ankles in stroke
140 patients. For the network analysis, we used a DCM-based Bayesian model selection to determine
141 (1) the relationships between the S1 and the motor network and (2) to identify the brain regions
142 that are handling the external stimulations. After the DCM model selection, we (3) investigated
143 the extrinsic connection strength differences between the two CPMs and (4) the dissimilarity of
144 the hemodynamic characteristics of brain regions belonging to the investigated networks.
145 Note that in contrast to most DCM studies, we leveraged the ability to make inferences about
146 neuronal and hemodynamic coupling. This is particularly prescient in the context of stroke
147 research, where lesions can produce both neuronal and neurovascular disconnections.
148

Materials & Methods

150 2.1. Subjects
151 Ten stroke patients (mean time of stroke: 18.2 days (SD = 11.4); mean age: 64 years (SD = 7.2);
152 female/male distribution: 5/5) were selected from a therapeutic study (Vér et al., 2016). Patient
153 data, location of the lesion, and National Institutes of Health Stroke Scale (NIHSS) scores are
154 summarized in Table 1. Each patient provided written informed consent prior to participation.
155
156 Table 1.
157
158 Due to ischemic stroke, patients had moderate or severe lower limb paresis. In our previous
159 study (Vér et al., 2016), we applied the NIHSS to assess the functional state and the severity of

160   the stroke in the patients. NIHSS is one of the most commonly used scales in the clinical field;
161   increasing scores indicate less functional states of the patients (Brott et al., 1989). Table 2 shows
162   the definitions of mild, moderate and severe paresis.
163   The inclusion criteria were ischemic stroke confirmed via clinical investigations and computed
164   tomography (CT). We selected subacute stage patients who were less than 30 days post-stroke.
165   Pavlova et al. defined acute stage 1 day to 1 week, subacute stage 1 week to 1 month and chronic
166   stage is more than 1 month after stroke (Pavlova et al., 2019).
167   Ability to cooperate during the MRI measurement was an inclusion criterion.
168   This study was approved by the Regional and Institutional Research Ethics Committee of the
169   Scientific Committee of the University of Debrecen, Clinical Center (DE OEC RKEB / IKEB
170   3772-2012; DE OEC RKEB / IKEB 3983–2013).
171
172   Table 2.
173
174   2.2. Functional Magnetic Resonance Imaging
175   Functional and structural images were acquired at the Kenézy University Hospital, Debrecen,
176   Hungary using a 1.5 Tesla Siemens Magnetom Essenza MR scanner. After the 3D T1-weighted
177   MP-RAGE structural image acquisition (TE=4.73 ms, TR=1540 ms, TI=800 ms, flip angle=15
178   slices with 0.9x0.9x0.9 mm voxels) two series of functional whole-brain images were obtained
179   for every subject using a BOLD contrast sensitive gradient-echo echo-planar sequence (TE=42
180   ms, flip angle=90, in-plane resolution=3x3mm; volume TR=4000 ms, axial slice thickness=3.3
181   mm). The two series involved the task of passive movement of the left or the right ankle
182   separately. Both series comprised 100 volumes that lasted 400 seconds containing 40 s-long
183   blocks of active and inactive periods. Following an initial resting period, active and inactive
184   blocks alternated throughout the session. During the inactive blocks, no stimulus was applied,
185   whereas in the active blocks, slow (~1Hz) continuous passive movement (CPM) of the left or
186   right ankle was performed by the physiotherapist. The legs and the hip of the patients were
187   fastened to the bed.
188
189
190
191   2.3. Data Analysis
192
193   2.3.1. Image Preprocessing
194   Before preprocessing, the left and the right sides of the structural and functional images of
195   patients with left hemispheric lesion were mirrored. This step facilitated a pooled population-
196   level statistical analysis for all the patients and prevented the need to split the population into two
197   cohorts depending on the side of the stroke.
198   The image processing pipeline followed the steps used in previous DCM studies regarding motor
199   control in stroke patients (Grefkes et al., 2008; Saleh et al., 2016). To erase non-brain areas from

200   the functional and structural scans, the brain extraction tool (BET) of FSL was used (Smith,
201   2002). The high resolution, brain extracted T1 images were spatially standardized to match the
202   symmetric template of MNI152 space (Grabner et al., 2006) using the linear and non-linear
203   registration utilities of the FSL package (Jenkinson et al., 2012). We verified the correctness of
204   the image transformation results via visual inspection.
205   For further analysis, the first three volumes of each functional dataset were excluded to avoid the
206   equilibrium effect of T1 images. The fMRI images were motion-corrected with the MCFLIRT
207   utility of FSL software (Jenkinson et al., 2000). The same software was applied to extract the six
208   motion parameters (three rotations and three translation components of rigid body
209   transformations). The fMRI data were then co-registered to the extracted anatomical brain image
210   and spatially transformed to MNI152 space using the deformation field obtained from the T1
211   standardization process.
212   On the functional images, we applied an isotropic Gaussian smoothing with 8 mm full width half
213   maximum (FWHM).
214
215   2.3.2. Independent Component Analysis
216   After independent component analysis (ICA) (Jung et al., 2001), we selected components
217   corresponding to motor network areas (M1, PM, and SMA) after visual inspection of the
218   statistical Student-t maps and characteristic time-series of the components on individual level.
219   We completed this search by identifying the primary somatosensory cortex (S1) to examine the
220   effects of the touching of the patients' legs by the physiotherapist during the passive movement
221   task. S1 is responsible for delivering information about the stimulation of the skin, the intestinal
222   mucous membrane of the internal organs, and about the position of the body parts (Borich et al.,
223   2015). We chose the highest z value within each cluster as the centre of the regions used in
224   DCM analysis.
225
226   2.4. Dynamic Causal Modeling
227   DCM is used to describe the causative structure of coupled dynamic systems. Using the
228   observable phenomenon of functional connectivity, which can be measured by correlations, for
229   example, and a special model that describes the observed statistical dependencies, we can map
230   the relationships between different brain areas.
231   We used a stochastic variant of the DCM algorithm (Li et al., 2011) that accommodates
232   endogenous or random fluctuations in hidden neuronal states. This variant is useful in most cases
233   because modelling state-noise is challenging. Allowing for random neuronal fluctuations results
234   in an estimation scheme more robust to model misspecification. A drawback of this method
235   compared to the original deterministic DCM is that the parameter estimation procedure, also
236   referred to as model inversion is much more computationally demanding. To limit the parameters
237   with which connection strength can be estimated, we restricted our DCM model space to
238   combine extrinsic connections and direct stimulating effects on brain regions.
239

240   2.5. Systematic Building of Model-Space

241   For building a DCM model-space for both fMRI sessions, we created bilateral models in relation

242   to the contralateral and ipsilateral brain hemispheres to the moved limb. For finding the most

243   probable connectivity architectures in the motor network based on the measured data, we defined

244   a two-sided base model: the extrinsic (i.e., between-region) directed connectivity between PM,

245   SMA, and M1 regions were fully connected within both hemispheres, and inter-hemispheric

246   connections were set between the M1s and SMAs (Figure 1A). To investigate the connections

247   between S1 and other regions within both sides of the movement, we defined four possible

248   network extensions: (1) S1 does not connect with PM, SMA and M1; (2) S1 only connects to

249   M1; (3) S1 only connects to PM; and (4) S1 connects to PM and M1 (Figure 1B, columns). For

250   checking the target regions of the external stimulus at the contralateral side of movement, we

251   considered three functional variations: (1) the stimulus directed to the PM and S1; (2) the

252   stimulus directed to the PM, S1, and M1; and (3) the stimulus directed to the S1 and M1 (Figure

253   1B, rows). Combining these possibilities, we established a model space comprising 4x3 = 12

254   model variants (Model1, Model2, - ..., Model12), which were arranged into a matrix form

255   (Figure 1B), to emphasize the factorial structure of this model space. The row view of this

256   arrangement represents the first model family set containing three model families (FS11, FS12,

257   and FS13) concerning the direct stimulus effect variants. The column view of this matrix shows

258   the second model family set consisting of four families according to the S1 connection

259   arrangements (Fstim1, Fstim2, Fstim3, and Fstim4).

260   Figure 1C shows an example of the combination of the base model and Model 4.

261

262   Figure 1.

263

264

265   Statistical analysis of between-subject (i.e., group) effects was performed under the winning

266   model using (nonparametric) classical inference. The winning model was identified by pooling

267   the evidence for different models over all subjects studied.

268

269   2.6. Comparison of Model Families and Model Selection

270   We used a Bayesian model comparison (BMC) (Penny et al., 2010) technique on both model

271   family sets to assess the most probable combination of these connectivity parameters based on

272   the fMRI patient. BMC focuses on a model structure that is created by defining and building a

273   model space. Model space usually means a set of models, where each model assigns specific

274   endogenous connections. The BMC procedure determines the model that best describes how the

275   data are generated by computing the expected and exceedance probability of each model (Penny

276   et al., 2004; Stephan et al., 2009). Expected probability shows the probability that a given model

277   generated the measured data. Exceedance probability indicates the probability that a given model

278   is more likely than any other models in the comparison. After the two BMC calculations, we

279   identified the best model family from both family sets, and we considered the mutual model of
280   these selected families as the winning model, which can be described by the measured data.
281
282   2.7. Hemodynamic Parameters
283   Neuronal activity leads to fMRI data by a dynamic process characterized by a Balloon model
284   (Buxton et al., 1998) and BOLD signal model (Stephan et al., 2007) for each brain region. This
285   defines how changes in neuronal activity cause changes in blood oxygenation that are measured
286   with fMRI.
287   DCM not only investigates the connection system during the model inversion but also estimates
288   the regional hemodynamic parameters of the Balloon model: hemodynamic signal decay (D),
289   transit time (T), and the ratio of intra- and extra-vascular components of gradient echo-signal (E)
290   (Stephan et al., 2007). An increase in the signal decay (D) reduces the regional cerebral blood
291   flow (rCBF) response to any input and suppresses the undershoot. The effect of increasing transit
292   time (T) is to slow down the dynamics of the BOLD signal regarding to the flow changes. The
293   parameter E reflects the efficacy of the following synaptic activity to generate the signal and the
294   potency of the stimulus in obtaining a neuronal response (Friston et al., 2000).
295   In this study, we examined the hemodynamic parameters in subacute stroke patients calculated
296   by the DCM of the winning model for statistical analysis.
297
298   2.8. Statistical Analysis
299   Because the non-paretic and paretic ankle CPMs induced lateralized brain activations, we had to
300   relabel the brain regions' names in the point of view of their laterality before statistical analysis.
301   Therefore, we used the ipsi-, and contralateral nomenclature (noted by i and c prefixes,
302   respectively) as Rehme and Saleh (Rehme et al., 2011; Saleh et al., 2016) used for denoting the
303   position of brain regions relative to the two types of stimuli, i.e., cM1, cSMA, cPM, cS1 and
304   iM1, iSMA, iPM, iS1. This allowed us to compare the connectivity strengths and hemodynamic
305   parameters of the activated (or passive) regions during the CPMs of the paretic and the non-
306   paretic ankles.
307   The expected distributions of the self-inhibition and inter-regional connections are different,
308   because self-connections are log scaling parameters of a negative a priori value (-0.5 Hz) to
309   ensure system stability in DCM, while extrinsic connections are not scaled and have a prior
310   expectation of 0 Hz. Thus, we separately investigated the normality of data using the Shapiro-
311   Wilk tests. Because these tests showed non-normality, we performed a mass of Monte-Carlo-
312   based exact permutation tests to statistically characterize the stimulus-related differences
313   between the paretic and non-paretic ankles in the elements of the endogenous connectivity
314   matrix (matrix A) and the parameters of modulatory effects (matrix B). Similarly, neither
315   external stimulus strength (matrix C) nor hemodynamic parameters were found normal
316   distribution, so we applied the same comparison technique for these data.
317   To correct for multiple comparisons, we applied the false discovery rate (FDR) for adjusting p-
318   values (Benjamini & Yekutieli, 2001) calculated by the statistical tests.

319

Results

320 **Results**
321 Using BMC selection, we found that during the CPM task, the S1 connection with the M1 and
322 PM (F^{S1}_4 family) was the most-likely network topology with 0.784 expected probability and
323 0.998 exceedance probability (Figure 2A/B). For direct effect model family selection, we
324 observed that the stimulus driving S1, M1 and PM (F^{stim}_2 family) was the most probable model
325 with 0.845 expected probability and 0.999 exceedance probability (Figure 2C/D). Using these
326 results, we selected Model11 (Figure 3) as the winning model for the statistical analysis.

327

328 Figure 2.
329 Figure 3.

330

331 As the Shapiro-Wilk tests resulted in p < 0.001 values in all datasets, we used Monte-Carlo-
332 based exact permutation tests in all connectivity and hemodynamic parameter comparisons.
333 Following the statistical analysis of the endogenous connectivity matrix of the winning model
334 (Model 11), we summarized the results in Table 3.

335

336 Table 3.

337

338 Using the FDR-corrected p-values (pFDR), we concluded that three contralateral self-inhibitions
339 (cM1, cS1, and cSMA), one contralateral inter-regional connection (cSMA→cM1), and one
340 interhemispheric connection (cM1→iM1) were significantly different during the comparison of
341 the two CPMs (Figure 4).

342

343 Figure 4.

344

345 Comparing the mean values, we showed that the paretic CPM caused stronger self-inhibition in
346 cM1 and cS1 and weaker self-inhibition in SMA (Figures 5A-C). The connection between
347 cSMA and cM1 dramatically changed (Figure 5D): during the non-paretic CPM, the cSMA
348 excited the neural activity of cM1, which in turn inhibited the paretic stimulus. The inter-
349 hemispheric cM1→iM1 connection shown showed stronger excitation during the paretic CPM in
350 relative to the non-paretic ankle's movement (Figure 5E).

351

352 Figure 5.

353

354   The statistical examination did not show any significant differences neither in the analysis of the
355 external stimulus (matrix C) or in the Balloon model parameter comparisons.

356

357

358

Discussion

360

361 In this work, we examined the connection topology of the S1-extended motor network and
362 investigated the differences in passive-movement related effective connectivity between the
363 paretic and non-paretic limbs during CPM in subacute stroke patients. As the exact effective
364 connectivity structure of the motor network in stroke is not well known, we applied an fMRI-
365 based model-search procedure to identify the model family that best fits the motor network
366 (Kahan & Foltynie, 2013; Penny et al., 2010). According to previous research, in this study, we
367 used the DCM-based effective connectivity technique to describe the motor network properties
368 during the applied CPM stimulations. We chose this method because it helps to understand the
369 causal architecture of the modelled networks by considering the temporal variation in the neural
370 activity estimated by the BOLD signal. We have used a conservative approach to compare
371 extrinsic connectivity between paretic and non-paretic stimulations of the investigated patient
372 group. This nonparametric approach to classical inference at the between-subject level is
373 conservative because it tests for differences in each connection separately (using FDR to adjust
374 for multiple comparisons). We could have used a multivariate test (e.g., canonical covariates
375 analysis). This would have been more sensitive and would have highlighted significant
376 stimulation differences. However, we would not have been able to assign a unique FDR's q
377 value to each connection. Finally, it should be noted that more recent analyses of between-
378 subject effects on effective connectivity in dynamic causal modelling would normally use
379 parametric empirical Bayes (Friston et al., 2016; Kass & Steffey, 1989). However, our classical
380 inference is sufficient for our purposes – and represents a simple way of accommodating
381 between-subject random effects.
382 For model selection, we defined two model families containing four and three models according
383 to the model-combinations of the S1 connections and the external stimuli modelling,
384 respectively. The applied BMC selection showed that the external sensory stimulation bound to
385 the S1 and PM regions, and the S1 had causal connections only with M1 and PM. A model-
386 family-based Bayesian model selection was also applied by Saleh et al. (Saleh et al., 2016), who
387 examined the interactions between regions that may modulate the activation of the ipsilesional
388 motor cortex during visual mirror feedback of unaffected hand movement in stroke patients.
389 They also identified a non-fully connected topological scheme as the best model.
390 After statistical comparison of the extrinsic connections of the winning model during the non-
391 paretic and paretic CPM, we concluded that three contralateral self-inhibitions (cM1, cS1, and
392 cSMA), one contralateral inter-regional connection (cSMA→cM1), and one interhemispheric
393 connection (cM1→iM1) were significantly different. Some neuroimaging studies reported that
394 during the movement of stroke-affected paretic limbs, a significant neural activity could be
395 observed in the regions of the contralesional hemisphere (Calautti et al., 2007; Ma et al., 2015;
396 Lazaridou et al., 2013; Badillo, Vincent & Ciuciu, 2013; Ward et al., 2003). Nowak et al.
397 demonstrated that overactivity in contralesional M1 occurs early after stroke, affecting the
398 improvement of these brain regions after the vascular incident Nowak et al., 2008). Grefkes et al.

399   also showed that the time after stroke is an essential factor influencing brain motor network
400   analysis (Grefkes et al., 2008).
401   The human motor network in the hemispheres contains several parts, including the primary
402   motor cortex (M1), supplementary motor area (SMA) and premotor cortex (PMC), which
403   territories show ordered representation of the human body, called as the somatotopic
404   representation. All the parts of the above territories send collateral fibres into the another
405   hemispheres through the corpus callosum, which fibres reaches the same somatotopic territories
406   (homotopic regions) (van den Heuvel &, Hulshoff, 2010). However, anatomical connectivity shows
407   difference between the upper and lower extremities, e.g. the activation of $M1_{hand}$ inhibit the
408   contralateral $M1_{hand}$ territory, whereas the activation of $M1_{foot}$ accused facilitatory coupling in the
409   contralateral hemisphere (Volz et al., 2015). The SMA and PMC have strong input into the M1,
410   therefore this adjacent territories can enhance the motor output of M1 pyramidal cells (Dancause
411   et al., 2005; Dum et al., 2005). The primary somatosensory cortex (S1) also able to modify
412   peripheral movements independently (a small part of the corticospinal tract originating from the
413   S1) or dependently from M1 in healthy patients or in stroke survivors. Here the anatomical basis
414   is the U-fibers which caused a strong connectivity between the neighbouring gyruses (Borich et
415   al., 2015). According to human data the increased peripheral somatosensory inflow helps in the
416   reorganization of M1 after stroke (Borich et al., 2015). This connection between the M1 and S1,
417   the literature uses the sensorimotor synchronization (SMS).
418   The different SMA-M1 connection strength is a common finding in many motor-based DCM
419   studies (Ward et al., 2003; Wang et al., 2016; Moulton et al., 2017). This connectivity, present
420   for simple and complex tasks alike, has been attributed to the respective role of the SMA and M1
421   in voluntary upper limb movements (Moulton et al., 2017). Pool et al. (Pool et al., 2013) showed
422   that movements at higher frequencies are linked with a linear increase in neural coupling
423   strength, especially from contralateral SMA to contralateral M1. This result shows that SMA
424   cooperates with variations in hand motor performance. Based on this and our results, we
425   concluded that the same alteration occurs in the case of the lower limb. The order of magnitude
426   of the contralateral SMA→M1 connection was different in the two CPMs: the SMA increased
427   the neural activity of M1 by 0.085 Hz (sd: 0.0496 Hz) during the non-paretic side activation, this
428   effect altered to -0.0053 Hz (sd: 0.0845 Hz) in the opposite CPM, which means that this
429   interaction occurs only in the non-paretic case. Diekhoff-Krebs et al. (Diekhoff-Krebs et al.,
430   2017) tested the hypothesis that interindividual variability in behavioural responses to excitatory
431   repetitive transcranial magnetic stimulation (rTMS) in stroke patients and healthy control group
432   is related to interindividual differences in the network connections of the stimulated region. Their
433   results revealed that a stronger connection exists between the SMA and the M1 regions before
434   intermittent theta-burst stimulation (iTBS) intervention at the affected arm in patients with better
435   motor performance. Our results support this statement because we also showed a strong
436   relationship between SMA and M1 regions.
437   The 50% stronger cM1-iM1 interaction (0.2761 Hz vs 0.1705 Hz) during the paretic CPM may
438   indicate a partial adaptive compensation for the injured motor cortex by the non-affected M1

439   after stroke. Most previous studies examined the functions of the upper limb after stroke. Grefkes
440   et al. showed that the inhibitory influences on movements of the paretic hand from the
441   contralesional to the ipsilesional M1 correspond with the degree of motor disability (Grefkes et
442   al., 2008). They recommended that the motor loss of patients with a single subcortical lesion is
443   connected to pathological interhemispheric interactions between the main motor regions. This
444   can be explained why we found a difference between interhemispheric connections. The
445   observed connectivity differences suggesting that the differences are region-specific, a residual
446   uncertainty as to localization remains, that is deep-rooted to cytoarchitectonic probability maps.
447   Functional connectivity studies have been conducted in stroke yet, the changes in tissue
448   composition at the site of the lesion is at various stages of necrosis and gliosis, affecting the
449   BOLD signal (Frias et al, 2018). It cannot be excluded that the change in tissue composition
450   might have an effect on functional connectivity. Our results demonstrate that stroke can affect
451   the functional connectivity of regions distant to the infarct, specifically S1, potentially further
452   compromising motor performance.
453   We showed that the hemodynamical parameters (Balloon model's D, T, and E) of the regions of
454   the motor networks were statistically similar during the two stimulations. This result suggests
455   that the detected differences in the connection strengths originated from real neural activity, and
456   the hemodynamic change had no confounding effect during the measurements.
457   Stroke recovery is a complex mechanism that possibly the results of substitution, compensation
458   of functions and combination of restoration (Hara, 2015). Many studies addressed the recovery
459   of motor skills after an intervention procedure, and it is well documented that the healthy brain
460   regions take over the functioning of the damaged areas (Jiang, Xu & Yu, 2013; Brown et al.,
461   2009). In a study on motor recovery following rehabilitation, Arya et al. (Arya et al., 2011)
462   proposed that the recovery could be compensatory motor recovery or real motor recovery, which
463   occurs when different connections that are unharmed send instructions to the same damaged
464   muscles to perform the motor orders. Neuronal reorganization and plasticity after a stroke takes
465   place during the first 6 months following stroke and involve brain regions distant to the affected
466   area (Li, 2017). According to Zeiler et al. after ischemic stroke, both spontaneous and
467   intervention-mediated recovery from impairment is maximal within 1-3 months (Zeiler et al.,
468   2013). Therefore it is difficult to interpret the outcomes of rehabilitative studies in human stroke
469   patients (Hara, 2015).
470
471

472   **Limitations and conclusion**

473
474   One limitation of the present study concerns the small sample size. We found significant changes
475   in effective connectivity despite the low number of patients. Furthermore, the difference between
476   left- or right-sided injuries or the anatomical regions of structural damage on effective
477   connectivity could be better investigated in studies with more extended groups.

478 Another limitation of this study is related to spontaneous plasticity recovery which takes place in
479 the early post-stroke period. Physiotherapy strategies used during the recovery process affect
480 spontaneous neuroplasticity. According to further studies, the optimal timing to begin
481 rehabilitation after stroke is still not known and it is highly possible that early intervening to
482 impacts cortical reorganization in a beneficial way (Coleman at al., 2017; Cassidy & Cramer,
483 2017).
484 In summary, our results confirm that the DCM-based connectivity analyses combined with
485 Bayesian model selection may be a useful technique for quantifying the alteration or differences
486 in the characteristics of the motor network in subacute stage stroke patients and in determining
487 the degree of MNW changes. However, in stroke, the number of patients who can be involved in
488 these types of fMRI studies is a severely limiting factor, yet.
489

Acknowledgements

491 This research was supported by the National Brain Research Program (2017-1.2.1-NKP-2017-
492 00002). There was no additional external funding received for this study.
493

References

495 Altamura C., Reinhard M., Vry M.S., Kaller C.P., Hamzei F., Vernieri F., Rossini P.M.,
496 Hetzel A., Weiller C., Saur D. 2009. The longitudinal changes of BOLD response and cerebral
497 hemodynamics from acute to subacute stroke. A fMRI and TCD study. BMC Neurosci. 10: 151.
498 DOI: 10.1186/1471-2202-10-151.
499

500 Aranyi C., Opposits G., Nagy M., Berényi E., Vér C., Csiba L., Katona P., Spisák T., Emri M.
501 Population-Level Correction of Systematic Motion Artifacts in fMRI in Patients with Ischemic
502 Stroke. 2017. J. Neuroimaging 27: 397-408. DOI: 10.1111/jon.12408.
503

504 Arya K.N., Pandian S., Verma R., Garg R.K. 2011. Movement therapy induced neural
505 reorganization and motor recovery in stroke: a review. J. Bodyw. Mov. Ther. 15: 528-37. DOI:
506 10.1016/j.jbmt.2011.01.023.
507

508 Badillo S., Vincent T., Ciuciu P. 2013. Group-level impacts of within- and between-subject
509 hemodynamic variability in fMRI. Neuroimage 82: 433-48. DOI:
510 10.1016/j.neuroimage.2013.05.100.
511

512 Bajaj S., Housley S.N., Wu D., Dhamala M., James G.A., Butler A.J. 2016. Dominance of the
513 Unaffected Hemisphere Motor Network and Its Role in the Behavior of Chronic Stroke
514 Survivors. Front. Hum. Neurosci. 10: 650. DOI: 10.3389/fnhum.2016.00650.
515

516 Benjamini Y., Yekutieli D. 2001. The control of the false discovery rate in multiple testing under
517 dependency. Annals of Statistics 29, 1165–1188. DOI: 10.2307/2674075.

518

519   Binkofsk F., Seitz R.J. 2004. Modulation of the BOLD-response in early recovery from
520   sensorimotor stroke. Neurology 63: 1223-9.

521

522   Biswal B., Yetkin F.Z., Haughton V.M., Hyde J.S. 1995. Functional connectivity in the motor
523   cortex of resting human brain using echo-planar MRI. Magn. Reson. Med. 34: 537-41.

524

525   Bonakdarpour B., Beeson P.M., DeMarco A.T., Rapcsak S.Z. 2015. Variability in blood oxygen
526   level dependent (BOLD) signal in patients with stroke-induced and primary progressive aphasia.
527   Neuroimage Clin. 8: 87–94. DOI: 10.1016/j.nicl.2015.03.014.

528

529   Bonakdarpour B., Parrish T.B., Thompson C.K. 2007. Hemodynamic response function in
530   patients with stroke-induced aphasia: Implications for fMRI data analysis. Neuroimage 36: 322–
531   331. DOI: 10.1016/j.neuroimage.2007.02.035.

532

533   Borich M.R., Brodie S.M., Gray W.A., Ionta S., Boyd L.A. 2015. Understanding the role of the
534   primary somatosensory cortex: Opportunities for rehabilitation. Neuropsychologia 79: 246-55.
535   DOI: 10.1016/j.neuropsychologia.2015.07.007.

536

537   Brott T., Adams H.P. Jr, Olinger C.P., Marler J.R., Barsan W.G., Biller J., Spilker J., Holleran
538   R., Eberle R., Hertzberg V., Rorick M., Moomaw C.J., Walker M. 1989. Measurements of acute
539   cerebral infarction: a clinical examination scale. Stroke 20: 864–870.

540

541   Brown C.E., Aminoltejari K., Erb H., Winship I.R., Murphy T.H. 2009. In vivo voltage-sensitive
542   dye imaging in adult mice reveals that somatosensory maps lost to stroke are replaced over
543   weeks by new structural and functional circuits with prolonged modes of activation within both
544   the peri-infarct zone and distant sites. J. Neurosci. 29: 1719-34.
545   DOI:https://doi.org/10.1523/JNEUROSCI.4249-08.2009.

546

547   Buxton R.B., Wong E.C., Frank L.R. 1998. Dynamics of blood flow and oxygenation changes
548   during brain activation: the balloon model. Magn. Reson. Med. 39, 855–864.

549

550   Calautti C., Naccarato M., Jones P.S., Sharma N., Day D.D., Carpenter A.T., Bullmore E.T.,
551   Warburton E.A., Baron J.C. 2007. The relationship between motor deficit and hemisphere
552   activation balance after stroke: a 3T fMRI study. Neuroimage 34: 322–331.

553

554   Cassidy J.M., Cramer S.C. 2017. Spontaneous and Therapeutic-Induced Mechanisms of
555   Functional Recovery After Stroke. Transl Stroke Res. 8: 33-46. DOI: 10.1007/s12975-016-0467-
556   5.

557

558   Cheng L., Wu Z., Fu Y., Miao F., Sun J., Tong S. 2012. Reorganization of functional brain
559   networks during the recovery of stroke: a functional MRI study. Conf. Proc. IEEE Eng. Med.
560   Biol. Soc. 4132-5. DOI: 10.1109/EMBC.2012.6346876.

561

562   Cleland B.T., Schindler-Ivens S. 2018. Brain Activation During Passive and Volitional Pedaling
563   After Stroke. Motor Control. 17: 1-29. DOI: 10.1123/mc.2017-0059.

564

565   Coleman E.R., Moudgal R., Lang K., Hyacinth H.I., Awosika O.O., Kissela B.M., Feng W.
566   2017. Early Rehabilitation After Stroke: a Narrative Review. Curr Atheroscler Rep. 19:59. DOI:
567   10.1007/s11883-017-0686-6.

568

569   Congdon P. 2007. Bayesian Statistical Modelling. Wiley.

570

571   Dąbrowski J., Czajka A., Zielińska-Turek J., Jaroszyński J., Furtak-Niczyporuk M., Mela A.,
572   Poniatowski Ł.A., Drop B., Dorobek M., Barcikowska-Kotowicz M., Ziemba A. 2019. Brain
573   Functional Reserve in the Context of Neuroplasticity after Stroke. Neural Plast. 27;
574   2019:9708905. DOI: 10.1155/2019/9708905.

575

576   Dancause N., Barbay S., Frost. S.B., Plautz E.J., Chen D., Zoubina E.V., Stowe A.M., Nudo R.J.
577   2005. Extensive cortical rewiring after brain injury. J. Neurosci. 25, 10167–10179. DOI:
578   10.1523/JNEUROSCI.3256-05.2005.

579

580   Diekhoff-Krebs S., Pool E.M., Sarfeld A.S., Rehme A.K., Eickhoff S.B., Fink G.R., Grefkes C.
581   2017. Interindividual differences in motor network connectivity and behavioral response to iTBS
582   in stroke patients. Neuroimage Clin. 15: 559-571. DOI: 10.1016/j.nicl.2017.06.006.

583

584   Dum R.P., Strick P.L. 2005. Frontal lobe inputs to the digit representations of the motor areas on
585   the lateral surface of the hemisphere. J. Neurosci. 25, 1375–1386. DOI:
586   10.1523/JNEUROSCI.3902-04.2005.

587

588   Frías I., Starrs F., Gisiger T., Minuk J., Thiel A., Paquette C. Interhemispheric connectivity of
589   primary sensory cortex is associated with motor impairment after stroke. Sci. Rep. 2018, 8:
590   12601. DOI: 10.1038/s41598-018-29751-6.

591

592   Friston K.J., Harrison L., Penny W. 2003. Dynamic causal modelling. Neuroimage 19: 1273-
593   302.

594

595   Friston K.J., Mechelli A., Turner R., Price C.J. 2000. Nonlinear responses in fMRI: the Balloon
596   model, Volterra kernels, and other hemodynamics. Neuroimage 12: 466-77.

597

598 Friston K.J., Litvak V., Oswal A., Razi A., Stephan K.E., van Wijk B.C.M., Ziegler G., Zeidman
599 P. 2016. Bayesian model reduction and empirical Bayes for group (DCM) studies. Neuroimage.
600 128: 413-431. DOI: 10.1016/j.neuroimage.2015.11.015.
601
602 Grabner G., Janke A.L., Budge M.M., Smith D., Pruessner J., Collins D.L. 2006. Symmetric
603 atlasing and model based segmentation: an application to the hippocampus in older adults. Med.
604 Image Comput. Comput. Assist. Interv. 9: 58-66. DOI: 10.1007/11866763_8.
605
606 Grefkes C., Nowak D.A., Eickhoff S.B., Dafotakis M., Küst J., Karbe H., Fink GR. 2008.
607 Cortical connectivity after subcortical stroke assessed with functional magnetic resonance
608 imaging. Ann Neurol. 63: 236-46. DOI: 10.1002/ana.21228.
609
610 Hamzei F., Knab R., Weiller C., Rother J. 2003. The influence of extra-and intracranial artery
611 disease on the BOLD signal in fMRI. Neuroimage 20: 1393-9.
612
613 Hara Y. 2015. Brain Plasticity and Rehabilitation in Stroke Patients. Journal of Nippon Medical
614 School 82: 4–13. DOI: 10.1272/jnms.82.4.
615
616 He S.Q., Dum R.P., Strick P.L. 1993. Topographic organization of corticospinal projections from
617 the frontal lobe: motor areas on the lateral surface of the hemisphere. J Neurosci. 13: 952-80.
618
619 Hoshi E., Tanji J. 2000. Integration of target and body-part information in the premotor cortex
620 when planning action. Nature 408: 466-470.
621
622 Inman C.S., James G.A., Hamann S., Rajendra J.K., Pagnoni G., Butler A.J. 2012. Altered
623 resting-state effective connectivity of fronto-parietal motor control systems on the primary motor
624 network following stroke. NeuroImage 59: 227–37. DOI: 10.1016/j.neuroimage.2011.07.083.
625
626 Jaillard A., Martin C.D., Garambois K., Lebas J.F., Hommel M. 2005. Vicarious function within
627 the human primary motor cortex? A longitudinal fMRI stroke study. Brain 128: 1122-38.
628
629 Jenkinson M., Bannister P., Brady M., Smith S. 2000. Improved Optimisation for the Robust and
630 Accurate Linear Registration and Motion Correction of Brain Images. NeuroImage 17: 825-841.
631 DOI: 10.1016/s1053-8119(02)91132-8.
632
633 Jenkinson M., Beckmann C.F., Behrens T.E., Woolrich M.W., Smith S.M. 2012. FSL.
634 NeuroImage 62: 782-790. DOI: 10.1016/j.neuroimage.2011.09.015.
635
636 Jiang L., Xu H., Yu C. 2013. Brain connectivity plasticity in the motor network after ischemic
637 stroke. Neural Plast. 924192. DOI: 10.1155/2013/924192.

638

639 Jung T.P., Makeig S., McKeown M.J., Bell A.J., Lee T.W., Sejnowski T.J. 2001. Imaging Brain
640 Dynamics Using Independent Component Analysis. Proc. IEEE Inst. Electr. Electron Eng. 89:
641 1107-1122. DOI: 10.1109/5.939827.

642

643 Kahan J., Foltynie T. 2013. Understanding DCM: Ten simple rules for the clinician. NeuroImage
644 83: 542-549. DOI: 10.1016/j.neuroimage.2013.07.008.

645

646 Kass R.E., Steffey D. 1989. Approximate Bayesian Inference in Conditionally Independent
647 Hierarchical Models (Parametric Empirical Bayes Models). Journal of the American Statistical
648 Association 407: 717-726.

649

650 Lam T.K., Dawson D.R., Honjo K., Ross B., Binns M.A., Stuss D.T., Black S.E., Chen J.J.,
651 Levine B.T., Fujioka T., Chen J.L. 2018. Neural coupling between contralesional motor and
652 frontoparietal networks correlates with motor ability in individuals with chronic stroke. J.
653 Neurol. Sci. 384: 21-29. DOI: 10.1016/j.jns.2017.11.007.

654

655 Lazaridou A., Astrakas L., Mintzopoulos D., Khanchiceh A., Singhal A., Moskowitz M., Rosen
656 B., Tzika A. 2013. fMRI as a molecular imaging procedure for the functional reorganization of
657 motor systems in chronic stroke. Mol. Med. Rep. 3: 775-9. DOI: 10.3892/mmr.2013.1603.

658

659 Li B., Daunizeau J., Stephan K.E., Penny W., Hu D., Friston K. 2011. Generalised filtering and
660 stochastic DCM for fMRI. Neuroimage 58: 442-57. DOI: 10.1016/j.neuroimage.2011.01.085.

661

662 Li S. 2017. Spasticity, Motor Recovery, and Neural Plasticity after Stroke. Front Neurol. 8: 120.
663 DOI: 10.3389/fneur.2017.00120.

664

665 Ma L., Steinberg J.L., Cunningham K.A., Lane S.D., Kramer L.A., Narayana P.A., Kosten T.R.,
666 Bechara A., Moeller F.G. 2015. Inhibitory behavioral control: a stochastic dynamic causal
667 modeling study using network discovery analysis. Brain Connect. 5: 177-86. DOI:
668 10.1089/brain.2014.0275.

669

670 Ma L., Steinberg J.L., Moeller F.G., Johns S.E., Narayana P.A. 2015 Effect of cocaine
671 dependence on brain connections: clinical implications. Expert Rev Neurother. 15: 1307-19.
672 DOI: 10.1586/14737175.2015.1103183.

673

674

675

676 Mehta J.P., Verber M.D., Wieser J.A., Schmit B.D., Schindler-Ivens S.M. 2012. The effect of
677 movement rate and complexity on functional magnetic resonance signal change during pedaling.
678 Motor Control. 16: 158-75. DOI: 10.1123/mcj.16.2.158.
679

680 Moulton E., Galléa C., Kemlin C., Valabregue R., Maier M.A., Lindberg P., Rosso C. 2017.
681 Cerebello-Cortical Differences in Effective Connectivity of the Dominant and Non-dominant
682 Hand during a Visuomotor Paradigm of Grip Force Control. Front Hum Neurosci. 11: 511. DOI:
683 10.3389/fnhum.2017.00511.
684

685 Nowak D.A., Grefkes C., Dafotakis M., Eickhoff S., Küst J., Karbe H., Fink G.R. 2008. Effects
686 of low-frequency repetitive transcranial magnetic stimulation of the contralesional primary motor
687 cortex on movement kinematics and neural activity in subcortical stroke. Arch Neurol. 65: 741-7.
688 DOI: 10.1001/archneur.65.6.741.
689

690 Pavlova E.L., Semenov R.V., Guekht A.B. Effect of tDCS on Fine Motor Control of Patients in
691 Subacute and Chronic Post-Stroke Stages. 2019. J Mot Behav. 17: 1-13. DOI:
692 10.1080/00222895.2019.1639608.
693

694 Penfield W., Boldrey E. 1937. Somatic motor and sensory representation in the cerebral cortex of
695 man as studied by electrical stimulation. Brain 60: 389-443.
696

697 Penny W.D., Stephan K.E., Daunizeau J., Rosa M.J., Friston K.J., Schofield T.M., Leff A.P.
698 2010. Comparing families of dynamic causal models. PLoS Comput. Biol. 6: e1000709. DOI:
699 10.1371/journal.pcbi.1000709.
700

701 Penny W.D., Stephan K.E., Mechelli A., Friston K.J. 2004. Comparing dynamic causal models.
702 Neuroimage 22:1157-72. DOI: 10.1016/j.neuroimage.2004.03.026.
703

704 Pool E.M., Rehme A.K., Fink G.R., Eickhoff S.B., Grefkes C. 2013. Network dynamics engaged
705 in the modulation of motor behavior in healthy subjects. Neuroimage 82: 68-76. DOI:
706 10.1016/j.neuroimage.2013.05.123.
707

708 Rehme A.K., Eickhoff S.B., Wang L.E., Fink G.R., Grefkes C. 2011. Dynamic causal modeling
709 of cortical activity from the acute to the chronic stage after stroke. Neuroimage 55: 1147-58.
710 DOI: 10.1016/j.neuroimage.2011.01.014.
711

712 Roc A.C., Wang J., Ances B.M., Liebeskind D.S., Kasner S.E., Detre J.A. 2006. Altered
713 hemodynamics and regional cerebral blood flow in patients with hemodynamically significant
714 stenoses. Stroke 37: 382-7.
715

716 Röther J., Knab R., Hamzei F., Fiehler J., Reichenbach J.R., Büchel C., Weiller C. 2002.
717 Negative dip in BOLD fMRI is caused by blood flow oxygen consumption uncoupling in
718 humans. Neuroimage 15: 98-102.
719
720 Saleh S., Yarossi M., Manuweera T., Adamovich S., Tunik E. 2016. Network interactions
721 underlying mirror feedback in stroke: A dynamic causal modeling study. Neuroimage Clin. 13:
722 46-54. DOI: 10.1016/j.nicl.2016.11.012.
723
724 Seghier M.L., Zeidman P., Neufeld N.H., Leff A.P., Price C.J. 2010. Identifying abnormal
725 connectivity in patients using dynamic causal modeling of FMRI responses. Front Syst Neurosci.
726 4. pii: 142. DOI: 10.3389/fnsys.2010.00142
727
728 Smith S.M. 2002. Fast robust automated brain extraction. Human Brain Mapp. 17: 143-155.
729
730 Stephan K.E., Penny W.D., Daunizeau J., Moran R.J., Friston K.J. 2009. Bayesian model
731 selection for group studies. Neuroimage 46:1004-17. DOI: 10.1016/j.neuroimage.2009.03.025.
732
733 Stephan K.E., Weiskopf N., Drysdale P.M., Robinson P.A., Friston K.J. 2007. Comparing
734 hemodynamic models with DCM. Neuroimage 38: 387-401. DOI:
735 10.1016/j.neuroimage.2007.07.040.
736
737 Tanji J., Shima K. 1994. Role for supplementary motor area cells in planning several movements
738 ahead. Nature 371: 413-416.
739
740 van den Heuvel M.P., Hulshoff Pol H.E. 2010. Specific somatotopic organization of functional
741 connections of the primary motor network during resting state. Hum. Brain Mapp. 31: 631–644.
742 DOI: 10.1002/hbm.20893.
743
744 Vér C., Emri M., Spisák T., Berényi E., Kovács K., Katona P., Balkay L., Menyhárt L., Kardos
745 L., Csiba L. 2016. The Effect of Passive Movement for Paretic Ankle-Foot and Brain Activity in
746 Post-Stroke Patients. Eur. Neurol. 76: 132-142. DOI: 10.1159/000448033.
747
748 Vinehout K., Schmit B.D., Schindler-Ivens S. 2019. Lower Limb Task-Based Functional
749 Connectivity Is Altered in Stroke. Brain Connect. 9: 365-377. DOI: 10.1089/brain.2018.0640.
750
751 Volz L.J., Eickhoff S.B., Pool E.M., Fink G.R., Grefkes C. 2015. Differential modulation of
752 motor network connectivity during movements of the upper and lower limbs. Neuroimage 119:
753 44-53. DOI: 10.1016/j.neuroimage.2015.05.101.
754

755   Wang L., Zhang J., Zhang Y., Yan R., Liu H., Qiu M. 2016. Conditional Granger Causality

756   Analysis of Effective Connectivity during Motor Imagery and Motor Execution in Stroke

757   Patients. Biomed Res Int. 3870863. DOI: 10.1155/2016/3870863.

758

759   Ward N.S., Brown M.M., Thompson A.J., Frackowiak R.S. 2003. Neural correlates of outcome

760   after stroke: a cross-sectional fMRI study. Brain 126: 1430-48.

761

762   Zeiler S.R., Krakauer J.W. 2013. The interaction between training and plasticity in the poststroke

763   brain. Curr Opin Neurol. 26: 609-16. DOI: 10.1097/WCO.0000000000000025.

Demographics, pathology data of stroke patients, clinical characteristics and NIHSS scores.

1   Table 1. Demographics, pathology data of stroke patients, clinical characteristics and NIHSS scores.

Patient/ Gender	Age (years)	Lesion type and topography (by CT)	Time of stroke	Severity of lower limb paresis	NIHSS
1/Male	63	Cerebral infarct in right MCA region	1 Month	Left sided mild-moderate paresis	1
2/Female	65	Cerebral infarct in left MCA	1 Month	Right sided severe paresis	3
3/Female	62	Bilateral lacunar infarcts, no fresh lesion	1 Month	Right sided moderate paresis	3
4/Male	56	Cerebral infarct in right MCA region	1 Month	Left sided moderate paresis	3
5/Male	52	No fresh lesion	9 days	Left sided moderate paresis	3
6/Female	82	Hypodens lesions in right hemisphere	6 days	Left sided moderate paresis	2
7/Female	75	Cerebral infarct in left MCA, old cerebral infarct in right MCA region	12 days	Right sided mild paresis	2
8/Female	71	Lesions frontal horns and cella media in right hemisphere	11 days	Left sided moderate paresis	2
9/Male	59	No fresh lesion	5 days	Right sided mild paresis	1
10/Male	58	No fresh lesion, old lesions in basal ganglia	9 days	Left sided moderate paresis	2

2   NIHSS: National Institutes of Health Stroke Scale

Definitions of mild and moderate paresis and severe paresis (6th item of the National Institutes of Health Stroke Scale).

1   Table 2. Definitions of mild and moderate paresis and severe paresis (6th item of the National
2   Institutes of Health Stroke Scale)

Definition of mild and moderate paresis (6th item of NIHSS)	1 point	Drift; leg falls by the end of the 5-second period but does not hit the bed
	2 points	Some effort against gravity; leg falls to bed by 5 seconds but has some effort against gravity
Definition of severe paresis (6th item of NIHSS)	3 points	No effort against gravity; leg falls to bed immediately
	4 points	No movement

Summarized statistical table of intrinsic (endogenous) connection strength analysis of the winning model performed by Monte-Carlo-based exact permutation tests following False Discovery Rate (FDR) correction.

1 Table 3. Summarized statistical table of intrinsic (endogenous) connection strength analysis of the
2 winning model performed by Monte-Carlo-based exact permutation tests following False Discovery Rate
3 (FDR) correction.

Connections	Mean connection strength during **non-paretic** ankle movement	SD of connection strengths during non-paretic ankle movement	Mean connection strength during **paretic** ankle movement	SD of connection strengths during paretic ankle movement	p value	FDR corrected p value
cM1→cM1	**-0.0925**	**0.0227**	**-0.1389**	**0.0489**	**0.0119**	**0.0395**
cM1→cPM	0.0224	0.1058	0.1086	0.0742	0.0510	0.0756
cM1→cSMA	0.0903	0.1060	0.0636	0.1118	0.5905	0.3992
cM1→iM1	**0.1649**	**0.0438**	**0.2651**	**0.1101**	**0.0127**	**0.0395**
cPM→cM1	0.0174	0.0667	0.0648	0.0597	0.1069	0.1073
cPM→cPM	-0.1339	0.0295	-0.1051	0.0388	0.0778	0.0939
cPM→cSMA	0.1345	0.0896	0.0592	0.0671	0.0485	0.0744
cS1→cM1	0.03680	0.0361	0.0361	0.0514	0.9768	0.5236
cS1→cPM	-0.0168	0.0401	-0.0064	0.0694	0.726	0.4496
cS1→cS1	-0.1021	0.0281	-0.1688	0.0579	0.0045	0.0395
cSMA→cM1	**0.0886**	**0.0511**	**6.3100e-06**	**0.0871**	**0.0123**	**0.0395**
cSMA→cPM	0.244	0.1376	0.1206	0.1464	0.0690	0.0887
cSMA→cSMA	**-0.1780**	**0.0340**	**-0.1350**	**0.0336**	**0.0133**	**0.0395**
cSMA→iSMA	0.2755	0.0797	0.3023	0.0896	0.4771	0.3493
iM1→cM1	0.1752	0.0834	0.2795	0.1319	0.0488	0.0746
iM1→iM1	-0.1062	0.0287	-0.1303	0.0413	0.1447	0.1400
iM1→iPM	-0.0003	0.1588	0.0155	0.1001	0.7919	0.4712
iM1→iSMA	0.0727	0.0605	0.0932	0.0924	0.5682	0.3900
iPM→iM1	-0.0024	0.1094	-0.0237	0.0260	0.5641	0.3883
iPM→iPM	-0.1310	0.0517	-0.1332	0.0544	0.9277	0.5107
iPM→iSMA	0.0304	0.0757	0.1112	0.1245	0.0966	0.1031
iS1→iM1	0.0382	0.0849	0.0363	0.0716	0.9615	0.5197
iS1→iPM	-0.0414	0.1473	-0.0286	0.0712	0.8337	0.4840
iS1→iS1	-0.1870	0.0784	-0.1391	0.0473	0.1042	0.1063
iSMA→cSMA	0.3144	0.1231	0.2658	0.0669	0.2867	0.2439
iSMA→iM1	0.1054	0.0548	0.0262	0.0893	0.0274	0.0591

iSMA→iPM	0.1260	0.0971	0.1808	0.1623	0.3723	0.2952
iSMA→iSMA	-0.1316	0.0337	-0.1709	0.0393	0.0298	0.0615

4   SD: standard deviation
5   p: probability
6   c: contralateral
7   i: ipsilateral
8   M1: primary motor cortex
9   PM: premotor cortex
10   SMA: supplementary motor area
11   S1: primary somatosensory cortex

Figure 1

Model selection for motor network.

(A) Base model: two-way extrinsic (endogenous) connections between PM, SMA, and M1 regions in both hemispheres, and the non-paretic-side M1 and paretic-side M1 areas and non-paretic-side SMA and paretic-side SMA regions were connected. (B) Differences of Model variations organized by two families: The external inputs are shown in the rows, which was only considered on the contralateral side. The columns show the connection system between the S1 and the motor network. (C) An example of the combination of the base model and Model4.
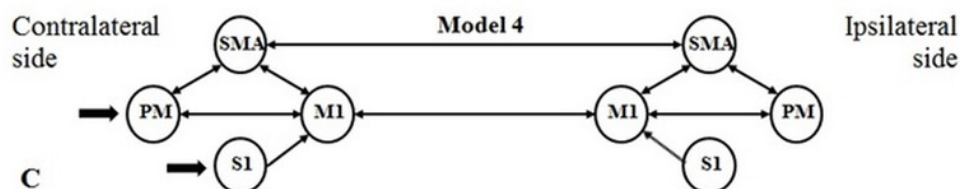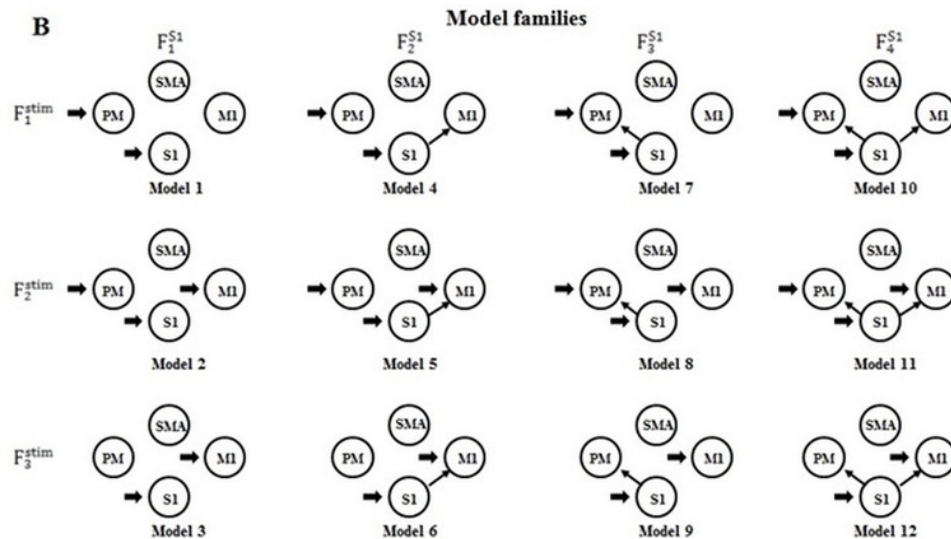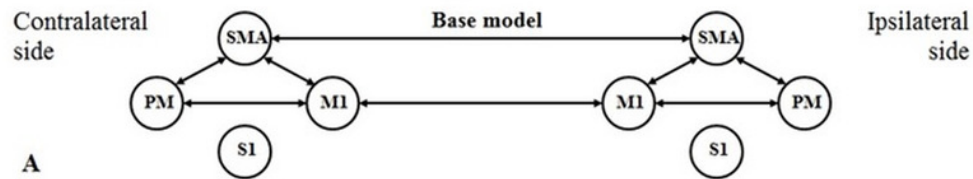
Figure 2

Results of the Bayesian Model Comparison (BMC) for the F^{S1} and F^{stim} model family sets.

Results of the Bayesian Model Comparison (BMC) for the F^{S1} and F^{stim} model family sets. Models of both non-paretic and paretic ankle continuous passive movement (CPM) was included in family-wise comparisons. The most probable network topology types were the F^{S1}_4 family, with expected probability (Exp_p) of 0.784 and exceedance probability (Exc_p) 0.998 (Panel A/B). For the direct effect model family selection, the F^{stim}_2 family was selected with 0.845 Exp_p and 0.999 Exc_p (Panel C/D).

A

Expected probability of 'S1' model families

B

Exceedance probability of 'S1' model families

C

Expected probability of 'stim' model families

D

Exceedance probability of 'stim' model families
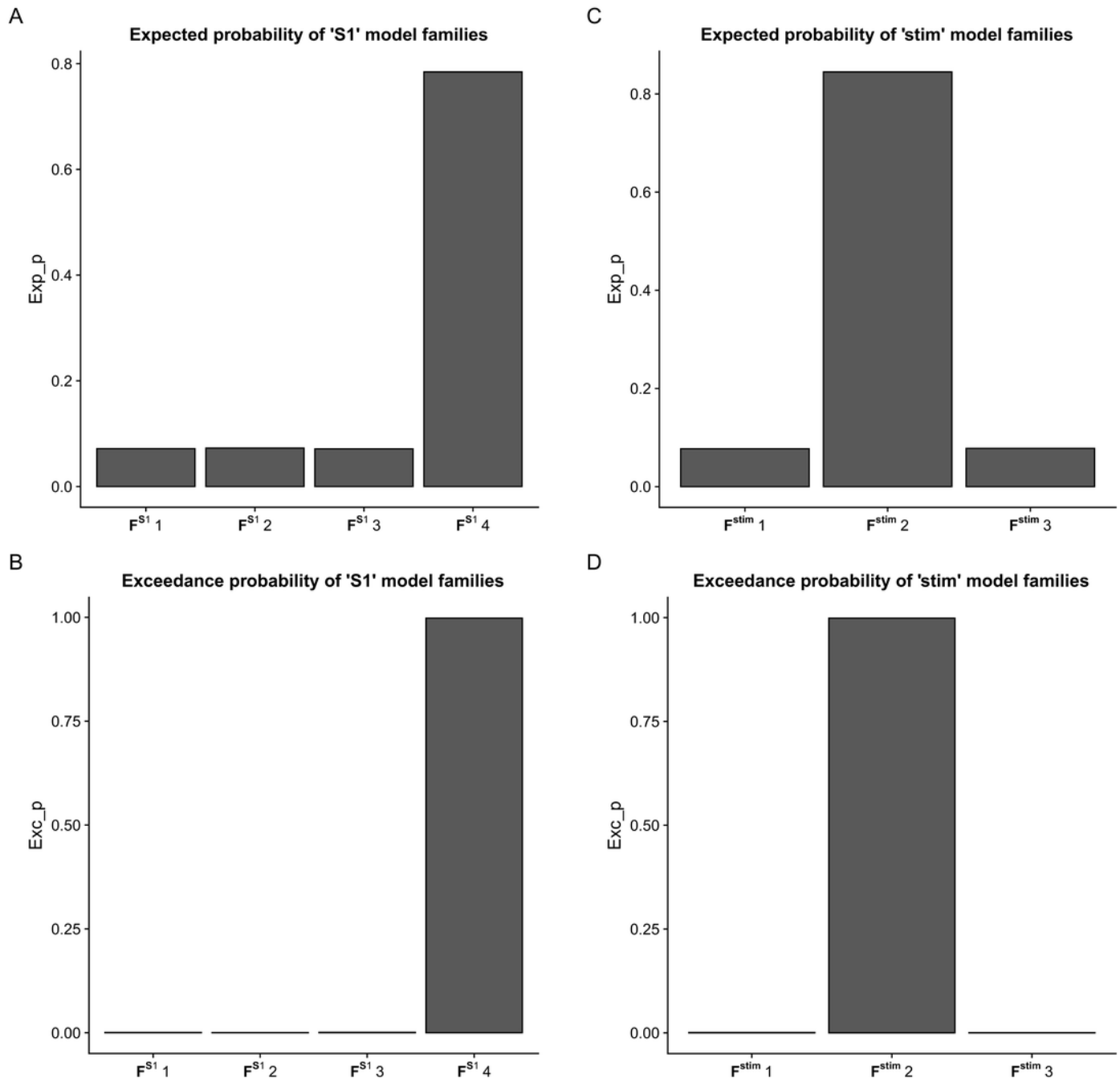
Figure 3

Comparison of model families.

Comparison of model families. (A) Base model: two-way extrinsic (endogenous) connections between PM, SMA, and M1 regions in both hemispheres, and the non-paretic-side M1 and paretic-side M1 areas and non-paretic-side SMA and paretic-side SMA regions were connected. (B) Panel B shows the 12 model variations organized in four F^{S1} families (columns) and three F^{stim} families (rows). Based on BMC results, we found that these models have the most evidence with the highest expected probability that connects S1 to both M1 and PM cortices (F^{S1}_4 denoted by - vertical grey rectangle). In the case of the direct effects of the stimulus changing between M1, PM, and S1 areas, the combination of all three regions provides the most probable pattern for stimulating the network for both the non-paretic and paretic sides (F^{stim}_2 denoted by - horizontal grey rectangle). Based on this the best model is Model 11, indicated by a grey rectangle.

Contralateral side

Base model

Ipsilateral side

A

Model families

F_1^{S1} Model 1

F_2^{S1} Model 4

F_3^{S1} Model 7

F_4^{S1} Model 10

F_1^{stim}

F_2^{stim} Model 2 · Model 5 · Model 8 · Model 11

F_3^{stim} Model 3 · Model 6 · Model 9 · Model 12

B
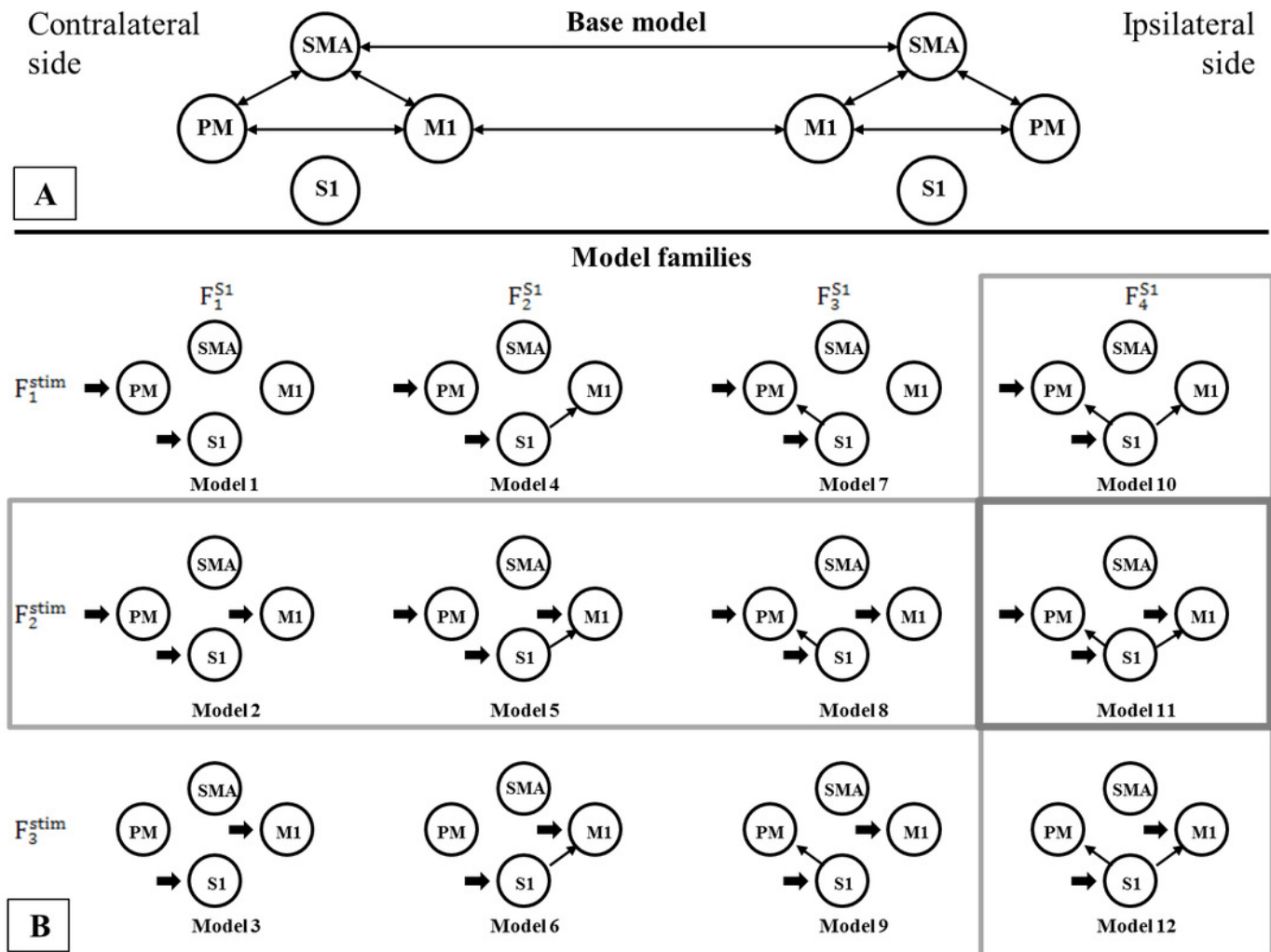
Figure 4

Mean values of significantly different endogenous connection (matrix A) strengths (see p-values in Table 3) of the best model (Model 11).

Bold arrows show the direction of significant connections. (A) Significant differences during non-paretic ankle movement: cSMA→cSMA (mean value = -0.18); cSMA→cM1 (mean value = 0.08); cM1→cM1 (mean value = -0.09); cM1→iM1 (mean value = 0.17) and cS1→cS1 (mean value = -0.10). (B) Significant differences during paretic ankle movement: cSMA→cSMA (mean value = -0.13); cSMA→cM1 (mean value = -0.005); cM1→cM1 (mean value = -0.14); cM1→iM1 (mean value = 0.27) and cS1→cS1 (mean value = -0.16). The empty arrows show the target location of external stimulus. The looping arrows represent the self-inhibitory effects.
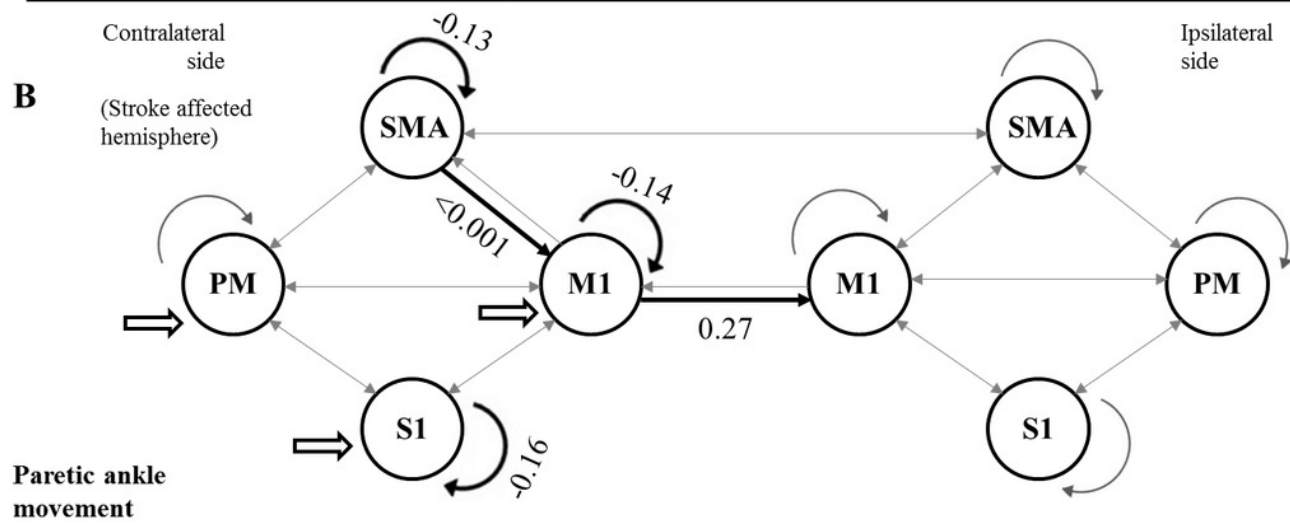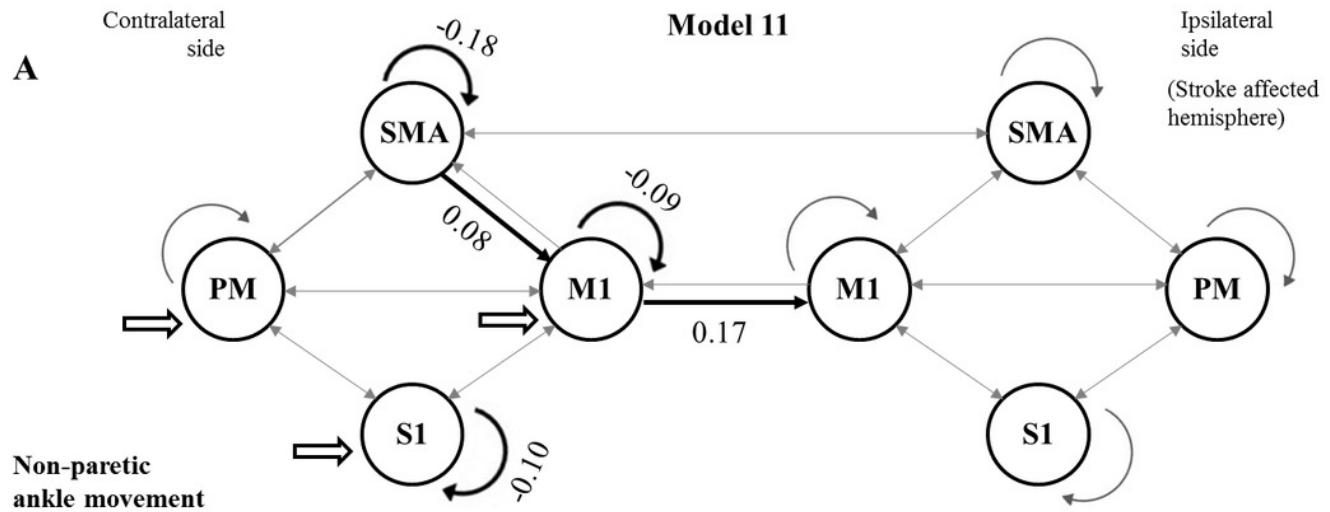
Figure 5

Comparison of mean values.

On the top of the images can be seen the FDR corrected p value differences between paretic and non-paretic ankle movement. (A) The paretic CPM caused stronger self-inhibition in cM1. (B) The paretic CPM caused stronger self-inhibition in cS1. (C) The paretic CPM caused weaker self-inhibition in SMA. (D) The cSMA→cM1 connection changed and, the cSMA excited the neural activity of cM1. (E) The cM1→iM1 connection showed stronger excitation during the paretic CPM.